 

# Mechanical properties of carbon nanotubes with vacancies and related defects

M. Sammalkorpi,[1,*] A. Krasheninnikov,[2] A. Kuronen,[1] K. Nordlund,[2] and K. Kaski[1]

[1] *Laboratory of Computational Engineering, Helsinki University of Technology, P.O.Box 9203, 02015 HUT, Finland*
[2] *Accelerator Laboratory, University of Helsinki, PO.Box 43, FIN 00014 University of Helsinki, Finland*

(Dated: August 13, 2004)

Although as-grown carbon nanotubes have relatively few defects, defects can appear at the purification stage or be deliberately introduced by irradiation with energetic particles or by chemical treatment when aiming at the desired functionality. The defects, especially vacancies, give also rise to a deleterious effect – deterioration of axial mechanical properties of nanotubes. By employing molecular dynamics simulations and continuum theory we study how the Young's modulus and tensile strength of nanotubes with vacancy-related defects depend on the concentration of defects and defect characteristics. We derive an analytical expression, with coefficients parametrized from atomistic computer simulations, which relates the Young's modulus and defect density in carbon nanotubes. We further show that the tensile strength and critical strain of single-walled nanotubes decrease by nearly a factor of two if an unreconstructed vacancy is present. However, this deterioration in the mechanical characteristics is partly alleviated by the ability of nanotubes to heal vacancies in the atomic network by saturating dangling bonds.

PACS numbers: 81.07.De, 61.80.Jh, 62.25.+g

## I. INTRODUCTION

Carbon nanotubes (CNTs) have extremely high axial Young's modulus of about 1 TPa [1–6] and tensile strength approaching 60 GPa [1, 7]. These exceptional mechanical properties along with low weight of CNTs and recent improvements in their synthesis and purification techniques make CNTs ideal candidates for reinforcement of various materials, *e.g.*, polymers [8–10]. High stiffness and tensile strength of CNTs should also provide mechanical stability for electric nano-circuits formed by CNTs with covalent inter-tube junctions [11].

These outstanding mechanical characteristics hold for nearly perfect CNTs. However, if CNTs have defects in the atomic network, one can expect that due to their quasi-one-dimensional atomic structure even a small number of defects will result in some degradation [12] of their characteristics. The defects can appear at the stage of CNT growth and purification [13, 14], or later on during device or composite production. Moreover, defects in CNTs can deliberately be created by chemical treatment [15] or by irradiation [11, 16–18] to achieve the desired functionality.

As an example of this, defects are expected to increase CNT adhesion to a polymer matrix [18, 19], which should result in improvements of the composite mechanical characteristics. Likewise, defects may enhance the overall characteristics of bundles of single-walled nanotubes (SWNTs) and multi-walled nanotubes (MWNTs). In these structures the interactions between intact nanotubes are governed by weak van der Waals forces, so that the axial mechanical load is carried only by the SWNTs at the rope perimeter [20] or by the outermost shell in MWNTs. Thus, creating strong defect-mediated covalent bonds between SWNTs in bundles [16, 17, 21–24] or between shells of MWNTs [25] by, for example, irradiation should provide load transfer to the inner tubes (shells). On the other hand, irradiation will create not only covalent bonds between the tubes but also defects in the atomic network.

Very recent experiments [24] on electron irradiation of carbon nanotube bundles followed by mechanical testing of the bundle bending modulus (which is proportional to the Young's modulus) indicate that small dose irradiation gives rise to a very large improvement in the mechanical properties of irradiated bundles. This result was understood in terms of irradiation-induced inter-tube links which provided load transfer and correspondingly enhanced the shear modulus inside the bundle. However, high-dose irradiation resulted in deterioration of mechanical characteristics due to accumulation of the irradiation-induced damage, and specifically vacancies, in the nanotube atomic network.

In addition to linking the nanotubes by covalent bonds, irradiation has experimentally been demonstrated to give rise to complete welding [11] and coalescence [26] of nanotubes thus opening new ways for electron/ion beam-assisted engineering of nano-circuits. The driving force for these structural transformations was found to be the formation of vacancies with chemically reactive dangling bonds followed by annealing of the damage in which the bonds were saturated. However, even spatially-localized irradiation will create defects not only in the junction region, but also in the rest of the system due to, *e.g.*, sputtered carbon atoms. This will inevitably result in deterioration of the mechanical stability of the system.

Therefore, to understand the role of defects in mechanical strength and to fully exploit the advantages potentially provided by the irradiation techniques, one should know how vacancy-related defects influence the mechan-

*Formerly M. Huhtala

ical characteristics of CNTs.

Although continuum methods [27–29] work well for perfect materials, they cannot directly be applied to nanotubes with defects, as these methods assume the material to be perfect. However, a combination of these methods and atomistic simulations can be used for evaluating elastic properties of nanotubes with defects, while only atomistic methods can be employed for simulating the plastic behavior. In this paper, by employing atomistic computer simulations and analytical continuum theory we study how the Young's modulus and tensile strength of CNTs depend on the concentration of vacancy-related defects. Since single and multi-vacancies might be present in post-processed nanotubes and because vacancies are the most prolific defects to appear due to both ion [30] and electron [31] irradiation, we concentrate on vacancies and related defects [30–33]. We consider only SWNTs as the behavior of MWNTs with vacancies under axial load can qualitatively be understood in terms of the data for SWNTs. We derive an expression which can be used to calculate the Young's modulus of defective CNTs at an arbitrary vacancy concentration. We also show that the ability of CNTs to heal vacancies in the atomic network by saturating dangling bonds partly alleviates the deterioration in their mechanical characteristics.

## II. COMPUTATIONAL METHODS

In our simulations, we used the classical molecular dynamics (MD) method [34] with the reactive analytical bond-order potential model parametrized by Brenner [35]. This model has widely been used in CNT simulations and a good agreement with the results obtained by *ab initio* methods have been reported [36, 37]. Berendsen temperature control method [38] was employed to describe the energy exchange with the heat bath. In our simulations of tensile strength we increased the onset of the interaction cut-off from 1.7 Å to 2.05 Å in order to avoid, at least partially, the overestimation of the force required to break a bond [39]. Other details of specific simulations are discussed in the corresponding sections.

## III. CONTINUUM MODEL FOR COMPUTING YOUNG'S MODULUS

In this section we derive an analytical expression for the Young's modulus of CNTs which can be used to estimate the Young's modulus as a function of the defect density. Then, in Section IV we fit the coefficients in the expression to reproduce the results of MD simulations at certain defect concentrations.

### A. Homogeneous material

The elastic energy $E(\varepsilon)$ of a body stretched in one direction can be written as

$$E(\varepsilon) = \frac{1}{2} Y_0 A L \varepsilon^2 = \gamma \varepsilon^2, \tag{1}$$

where $Y_0$ is the Young's modulus of the homogeneous body, $A$ is the cross section, $L$ is the length and $\varepsilon$ is the strain. The coefficient $\gamma$ can be determined by fitting it to reproduce the $E(\varepsilon)$ curve calculated through atomistic simulations. Then the Young's modulus can be expressed in terms of $\gamma$ as

$$Y_0 = \frac{2\gamma}{AL}. \tag{2}$$

Because of the tubular structure of the SWNT there is an ambiguity in determining the cross-section area $A$ of the nanotube. Formally the area can be written as $A = 2\pi r t$, where $r$ is the tube radius and $t$ the graphene layer thickness, leading to a Young's modulus $Y_0 = 2\gamma/2\pi r t L$. However, the thickness $t$ is not well defined because the layer is mono-atomic. Therefore we employ a definition of Young's modulus in which the normalization is not per unit cross sectional area but per unit cross sectional length:

$$Y_{s0} = \frac{2\gamma}{2\pi r L} = \frac{\gamma}{\pi r L}. \tag{3}$$

### B. Defective body

In the continuum treatment we divide the system of length $L$ into $N$ sections. As will be shown, the outcome is independent of the division details but it may help to visualize the division by splitting the tube into $N$ sections of equal length, for example nanotube unit cells. We assume here that the division can be made in such a way that each section contains no more than one defect, *i.e.*, for the defect concentration being relatively low. Each section $i$ is characterized by its defect type $\alpha_i$. Number of sections with defect $\alpha$ is denoted by $m_\alpha$ and the total number of different defect types is $M$. Further, each defect type $\alpha$ is characterized by its Young's modulus $Y_\alpha$ and section length $L_\alpha$. Defect type $\alpha = 0$ stands for an intact tube section and thus $L_0$ denotes the length of an elementary section without defects.

The total tube length can now be expressed either in terms of defect types or in terms of sections as follows

$$L = \sum_{\alpha=0}^{M} m_\alpha L_\alpha = \sum_{i=1}^{N} L_{\alpha_i}. \tag{4}$$

Analogously to Eq. 1 the elastic energy of a stretched defective body divided into $N$ sections can be written as

$$E = \frac{1}{2} Y A L \varepsilon^2 = \sum_{i=0}^{N} \frac{1}{2} Y_{\alpha_i} A L_{\alpha_i} \varepsilon_i^2, \tag{5}$$

where $Y$ is the Young's modulus of the whole body and $Y_{\alpha_i}$, $L_{\alpha_i}$ and $\varepsilon_i$ are Young's modulus, the equilibrium length and the strain of section $i$, respectively. When stretched, the strain for the whole body can be written as $\varepsilon = (\sum_{i=0}^{N} \ell_i - L)/L$ or for each section as $\varepsilon_i = (\ell_i - L_{\alpha_i})/L_{\alpha_i}$, where $\ell_i$ is the stretched length of section $i$. Consequently, the stretching force is

$$F = -\frac{YA}{L}\left(\sum_{i=0}^{N} \ell_i - L\right), \tag{6}$$

or, as the force acts equally on each of the sections (analogously to a system of springs in series),

$$F = -\frac{Y_{\alpha_i} A}{L_{\alpha_i}}(\ell_i - L_{\alpha_i}). \tag{7}$$

By multiplying both sides of the latter equation by $L_{\alpha_i}/Y_{\alpha_i} L$ we get

$$F\frac{L_{\alpha_i}}{Y_{\alpha_i} L} = -\frac{A}{L}(\ell_i - L_{\alpha_i}). \tag{8}$$

Finally, by summing over all the sections and applying Eq. 4 we arrive at

$$F = -\left(\sum_{i=0}^{N} \frac{L_{\alpha_i}}{Y_{\alpha_i} L}\right)^{-1} \frac{A}{L}\left(\sum_{i=0}^{N} \ell_i - L\right). \tag{9}$$

Then from the comparison to Eq. 6 we obtain the Young's modulus of the whole body as

$$Y = \left(\sum_{i=0}^{N} \frac{L_{\alpha_i}}{Y_{\alpha_i} L}\right)^{-1} \Leftrightarrow \frac{1}{Y} = \sum_{i=0}^{N} \frac{L_{\alpha_i}}{Y_{\alpha_i} L}. \tag{10}$$

This can be further simplified to the following form

$$\frac{Y_0}{Y} = \sum_{\alpha=0}^{M} \frac{m_\alpha L_\alpha}{L} \frac{Y_0}{Y_\alpha}, \tag{11}$$

where the terms corresponding to similar defect sections have been combined and the summation now goes over the $M$ different defect types ($\alpha = 0$ refers to intact tube sections). The expression relates the linear defect concentration $n_\alpha = m_\alpha/L$ and Young's modulus by

$$\frac{Y_0}{Y} = \frac{m_0 L_0}{L} + \sum_{\alpha=1}^{M} n_\alpha L_\alpha \frac{Y_0}{Y_\alpha}. \tag{12}$$

Now remembering that $Y_{s0}/Y_s = Y_0/Y$ and expressing the total length of intact sections as the difference between the total length and the length of the defective sections ($m_0 L_0 = L - \sum_{\alpha=1}^{M} m_\alpha L_\alpha$, Eq. 4), we obtain the final form of the defect concentration and Young's modulus relation:

$$\frac{Y_{s0}}{Y_s} = 1 + \sum_{\alpha=1}^{M} n_\alpha a_\alpha, \tag{13}$$

where

$$a_\alpha = L_\alpha\left(\frac{Y_0}{Y_\alpha} - 1\right) = L_\alpha\left(\frac{Y_{s0}}{Y_{s\alpha}} - 1\right). \tag{14}$$

The parameter $a_\alpha$ can be fitted to reproduce experimental or simulation data. We emphasize that the result is independent of how the division into tube sections is made. This can be seen by employing the formula recursively.

## IV. RESULTS AND DISCUSSION

### A. Young's modulus and tensile strength of intact nanotubes

In order to have a reference point for nanotubes with defects, we have first computed Young's moduli of perfect SWNTs. The results are presented in Table I. For the Young's modulus our simulations give a value of 0.7 TPa, insensitively to tube chirality and diameter. This is in line with the experimental values of CNT Young's modulus around 1 TPa [1, 2, 4, 7] and with previous simulations using the Brenner potential [28, 40, 41].

We have also evaluated the critical strain and tensile stress by fixing atoms at one end of the tube and applying a force that increases linearly in time to the other end until the tube breaks, see Fig. 1. The force is increased with a rate of 0.8 eVÅ$^{-1}$ps$^{-1}$. We have aimed to model the tube fracture at low temperatures (i.e. $T \sim 0$ K) but because the onset of the fracture requires fluctuations, the temperature was kept at 10 K.

The calculated critical strain and tensile strength are also listed in Table I. In accordance with other similar simulations [39, 40, 42], the values proved to be higher than the experimental values which approach 60 GPA for tensile strength [1, 7] and 12% for the yielding strain [7]. In part, this is due to the cut-off problem [39] typical for Tersoff-like potentials, for which the atomic interaction energy is artificially driven to zero at a certain separation between atoms. This in turn causes the corresponding inter-particle force to be overestimated, as can be seen from the force-strain curves with various cut-offs for a (5,5) nanotube given in Fig. 1. In order to circumvent this problem, we have increased the onset of interaction cut-off from 1.7 Å to 2.05 Å in the simulations.

From the curves of Fig. 1 it is seen that by increasing the cut-off we do not affect the force-strain curve at inter-particle distances shorter than the cut-off as long as the cut-off remains smaller than the distance to the second closest neighbor. We interpret the bond rupture force as the maximum force outside the cut-off peak region. The bond rupture point for a cut-off onset values of 1.9 Å and 2.05 Å is marked by 'X' in Fig. 1. In the case of 1.7 Å cut-off onset the artificial peak in force covers this point.

It is well known that the nanotube fracture behavior depends on temperature and simulation time as well the loading rate [39, 40, 42, 43]. We note that in this study

we did not account for possible formations of topological defects in strained nanotubes [44–46], because *ab initio* calculations indicate that the formation energy of these defects is very high [37, 47]. Finally, as we discuss below, one can expect that a small number of defects is always present in the nanotubes used for mechanical testing. We stress, however, no matter what the origin of the discrepancy between the absolute values of the experimental and calculated tensile strength is, in this work we are interested more in vacancy-mediated changes rather than in absolute values of tensile characteristics.

TABLE I: Young's modulus, critical strain $\varepsilon$ and tensile strength $\sigma$ of perfect nanotubes. $Y_{s0}$ refers to surface based Young's modulus and $Y_0$ to conventional Young's modulus (see Eqs. 2 and 3). The graphite interlayer distance $t = 3.35$ Å has been used as the thickness of a nanotube shell in computing $Y_0$ and $\sigma$.

| Tube | Diameter (Å) | $Y_{s0}$ (N/m) | $Y_0$ (GPa) | $\varepsilon$ | $\sigma$ (GPa) |
|---|---|---|---|---|---|
| (5,5) | 6.78 | 230 | 690 | 0.260 | 240 |
| (9,0) | 7.05 | 220 | 669 | 0.22 | 220 |
| (10,10) | 13.56 | 240 | 700 | 0.27 | 240 |
| (17,0) | 13.31 | 230 | 690 | 0.21 | 220 |

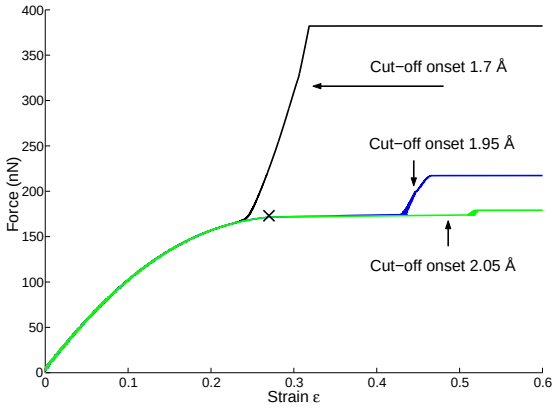


FIG. 1: Force-strain curves for an ideal (5,5)-nanotube at 10 K temperature with three different cut-off radii. The onset of the cut-off function can be perceived as an artificial peak. The flat regime depicts a sudden bond elongation to a length corresponding to the cut-off. Thus the beginning of this plateau, 'X', corresponds to the largest value of force outside the cut-off peak and will be interpreted as bond rupture.

### B. Vacancy-related defects on walls of carbon nanotubes

Vacancy-related defects can appear in nanotubes during purification or as a result of irradiation. In the latter case collisions of energetic particles – electrons or ions – with CNTs displace carbon atoms in the nanotube network from their original positions thus giving rise to vacancies in the graphitic shells and to carbon interstitials in the inter-tube regions. Energetic electrons produce mostly single vacancies by knocking out carbon atoms in the nanotube network [48], whereas heavy ions can easily give rise to multi-vacancies by sputtering several adjacent carbon atoms. These vacancies can transform into other vacancy-related defects by saturating some of the dangling bonds [30–33]. For a single vacancy, this reconstruction results in the appearance of a pentagon ring accompanied by the protrusion of the atom with a dangling bond by $0.5 - 0.7$ Å out of the plane, as in graphite [49]. Multi-vacancies reconstruct in more complex structures as described later.

It is intuitively clear that vacancies have a much stronger effect on the axial mechanical characteristics of individual SWNTs than interstitial atoms. Therefore, in this work we dwell only on vacancies. Assuming that the vacancies have been formed under irradiation, we simulated the response of defective SWNTs to axial mechanical load. We calculated the Young's modulus and tensile strength of four nanotubes with different chiral indices: (5,5)-, (9,0)-, (10,10)-, and (17,0)-tubes. These particular tube indices were chosen in order to observe the possible diameter and chirality effects.

We have considered SWNTs with a single vacancy (one atom removed), with a double vacancy (two adjacent atoms knocked out) and with a triple vacancy (three adjacent atoms missing), as depicted in Figs. 2(a-c). In what follows, these configurations will be referred to as non-reconstructed defects. In each tube the non-reconstructed double and triple vacancy defects have two axially distinguishable orientations separated by 120 degrees (only one configuration is shown in Fig. 2). These atomic configurations are metastable but can survive for macroscopic times at low temperatures [30, 32], or when the atoms with dangling bonds are bonded to a surrounding medium, *e.g.*, a polymer matrix.

The other type of defects studied here are the vacancy-related defects, *i.e.*, vacancies in SWNTs relaxed to the global minimum energy configuration. In order to find these low energy configurations, the non-reconstructed vacancies were thermally annealed at a temperature of 3000 K for 40 ps before the system was slowly cooled down at an average rate of 5 K/ps using the Berendsen thermostat [38]. These configurations are presented in Fig. 2(d-f) for (10,10) armchair tubes and in Fig. 2(g-i) for (17,0) zig-zag tubes. The vacancy configurations in the other studied SWNTs are similar to those shown in Fig. 2.

### C. Young's modulus of nanotubes with defects

We have calculated the Young's moduli of SWNTs with one vacancy but different tube lengths. These cor-

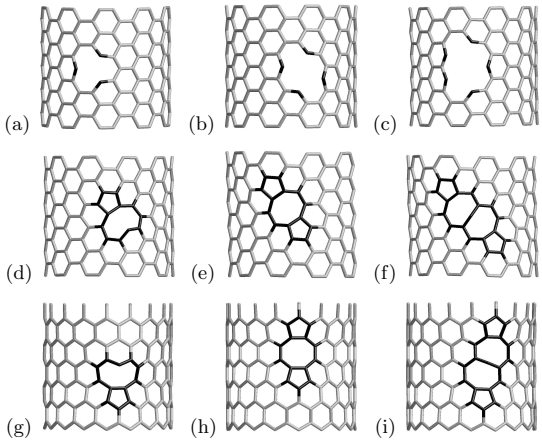


FIG. 2: Atomic networks of SWNTs with non-reconstructed (a-c) and reconstructed (d-i) single (a,d,g), double (b,e,h) and triple (c,f,i) vacancies. Only the front wall of each tube is shown. The bottom row configurations correspond to a (17,0) zig-zag SWNT, and the others to a (10,10) armchair SWNT.

respond to linear defect concentrations of 1/25 Å$^{-1}$ (one defect per 25 Å), 1/50 Å$^{-1}$, 1/100 Å$^{-1}$, 1/150 Å$^{-1}$, and 1/200 Å$^{-1}$. Both non-reconstructed and reconstructed vacancies were examined. The energy of a given structure was calculated as the tube length was increased from its non-stretched equilibrium value. Then the Young's modulus $Y_s$ was determined from the smooth curve fitted to the simulation points. The results are presented in the form of Eq. 13 (with $M = 1$) in Fig. 3, which presents the inverse of the scaled Young's modulus as a function of defect concentration for non-reconstructed and reconstructed vacancies. From this figure it is evident that the inverse scales linearly with the defect concentration, which validates the use of the continuum theory (Eq. 13). Different symbols refer to the type of the vacancy and are explained in the figure caption.

The data in Table II shows the dependency of the Young's modulus on the defect type, *i.e.*, the coefficients $a_\alpha$ for each defect type. As expected, single vacancies, whether reconstructed or non-reconstructed, decrease the Young's modulus least whereas the larger vacancies more. The reconstruction matters for double and triple vacancies but not so much for single vacancies. This can be understood in terms of the vacancy geometries presented in Fig. 2. The "hole size" for the reconstructed single vacancy is practically the same as before the reconstruction. Also, the difference between the behavior of thin (5,5) and (9,0) tubes and the thicker (10,10) and (17,0) tubes is as expected, *i.e.* the defective region is a much smaller portion of the tube circumference in the thicker tubes and therefore the Young's modulus is not so sensitive to the defects nor to the order of vacancy or reconstruction. Chirality dependence is observed only in the non-reconstructed vacancies because the axial orientation of higher order vacancies influences the result. In general reconstructed vacancies result in stiffer tubes than non-reconstructed but some orientations of non-reconstructed vacancies appear to affect the stiffness less than the corresponding reconstructed defects, especially for the larger tubes. The reason for this is that the relative decrease in the size of holes in reconstruction is smaller for the large tubes. Therefore, as the bonds of an atom with a dangling bond are stiffer than regular $sp^2$ bonds, a favorable local bond orientation in the non-reconstructed vacancy

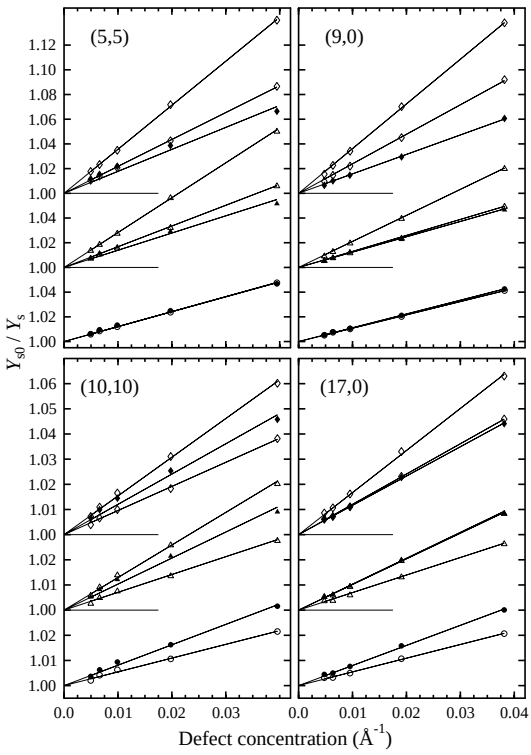


FIG. 3: Inverse of the scaled Young's modulus $Y_{s0}/Y_s$, (where $Y_{s0}$ is the surface based Young's modulus of a perfect tube) plotted as a function of the defect concentration (or $1/L$) for four different nanotubes with single, double and triple vacancies. Circles refer to single vacancies, triangles to double vacancies and diamonds to triple vacancies. Filled symbols stand for reconstructed defects, whereas open symbols are for non-reconstructed defects. Non-reconstructed double and triple vacancies have two possible axial orientations which result in different $Y_s$ behavior and two separate data sets. The lines have been obtained by fitting the continuum Eq. 13 (with $M = 1$) to each data set.

TABLE II: The coefficients $a_\alpha$ (Eq. 13) necessary to calculate the Young's modulus of a defective nanotube. The boldface numbers represent the $a_\alpha$ values corresponding to reconstructed vacancies and the values in parenthesis the non-reconstructed vacancies. The two numbers inside the parenthesis for the double and triple vacancies represent the two alternative orientations of the non-reconstructed defects. The Young's modulus for an arbitrary defect concentration can be computed by plugging in the values to Eq. 13.

| Tube | $Y_0$ | $a_1$ 1 atom missing | $a_2$ 2 atoms missing | $a_3$ 3 atoms missing |
|---|---|---|---|---|
| | (GPa) | (Å) | (Å) | (Å) |
| (5,5) | 690 | **1.2** (1.2) | **1.4** (1.7/2.8) | **1.8** (2.2/3.6) |
| (9,0) | 670 | **1.1** (1.1) | **1.2** (1.3/2.1) | **1.6** (2.4/3.6) |
| (10,10) | 700 | **0.8** (0.5) | **1.0** (0.7/1.3) | **1.2** (1.0/1.5) |
| (17,0) | 690 | **0.8** (0.5) | **1.0** (0.7/1.0) | **1.2** (1.2/1.7) |

may result in a stiffer tube than the reconstructed vacancy for small deflections.

The values of coefficients $a_\alpha$ provided in Table II can be used to compute the Young's modulus for an arbitrary defect concentration. For example, if we have $(5,5)$ nanotubes with single, double and triple vacancies with concentrations of $10^{-4}$Å$^{-2}$ or 1 defect every 50 Å for the single vacancies and $10^{-5}$Å$^{-2}$, that is 1/500 Å$^{-1}$, for the double and triple vacancies, Eq. 13 predicts the Young's modulus as

$$\begin{aligned} \frac{Y_0}{Y} &= 1 + a_1 n_1 + a_2 n_2 + a_3 n_3 \\ Y &= 0.97 Y_0. \end{aligned} \tag{15}$$

Essentially, these numbers show that the averaged defect concentration has to be very high to cause a noticeable decrease in the Young's modulus. Even for relatively high concentrations used in the example the decrease in the Young's modulus is predicted to be only about 3 %.

### D. Tensile strength of nanotubes with defects

In order to calculate the tensile strength and critical strain of nanotubes with defects, we have used the same simulation setup as for intact SWNTs. The results for defective structures are presented in Fig. 4 where the reduced critical strain $\tilde{\varepsilon} = \varepsilon/\varepsilon_0$ and the reduced tensile strength $\tilde{\sigma} = \sigma/\sigma_0$. Here $\varepsilon_0$ refers to the critical strain and $\sigma_0$ to the tensile strength of a pristine nanotube. The significance of defect reconstruction can be clearly seen – the tubes with reconstructed vacancies are much stronger than the tubes with non-reconstructed defects. The results are also chirality dependent, *i.e.* in zig-zag tubes the reconstruction heals the carbon network to almost ideal strength, ca. 95% of the critical strain and tensile strength in an ideal tube. Reconstructed single and double vacancies are equally strong within the presentation accuracy and the structure with a reconstructed triple vacancy is only slightly weaker. This can be understood if the stress concentration factor [50] of each defect type is considered. As visible in Fig. 2, if a zig-zag tube is loaded axially, the load spreads symmetrically on the defect region bonds. On the other hand, in the armchair case (see Fig. 2(d-f)) the load spreads unevenly on respective bonds, that is, the stress concentration factor is larger locally. Thus the corresponding bonds are the first to yield and result in critical strains of ca. 70% and tensile strengths of ca. $85-90$% of the perfect tube values.

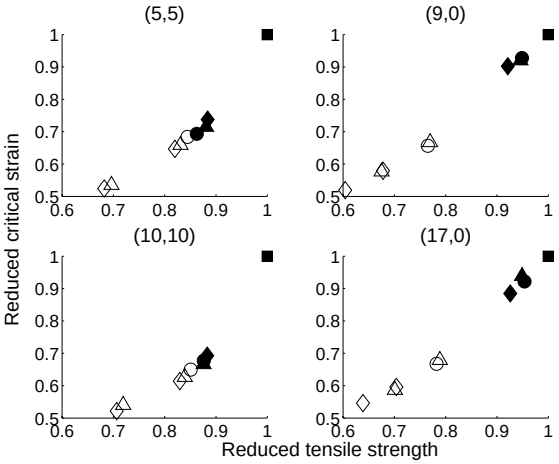


FIG. 4: Tensile strength and critical strain of nanotubes with defects. Filled symbols correspond to reconstructed vacancies and open symbols to non-reconstructed vacancies. Squares are the reference values for perfect tubes, circles stand for tubes with a monovacancy, triangles with a double vacancy and diamonds for tubes with a triple vacancy.

Non-reconstructed vacancies result in much lower tube strength. Thus, the significance of the defect size with respect to the tube circumference can be seen very clearly. For example, for armchair tubes the symbols in Fig. 4 corresponding to non-reconstructed single vacancy and one orientation of the double and triple vacancy clamp together around critical strain 65%, tensile strength 85%. The reason for this, again, is the stress concentration factor. These symbols correspond to vacancies shown in Fig. 2(a-c). If any of these configurations is viewed in the axial direction, the portions of defective cross-circumference are identical and the stress concentration factors are equal because of axially similar bond orientations in the defect region. The single vacancy is slightly stronger than the double vacancy, which on the other hand exceeds the triple vacancy in strength. This is because fracture is an activated process and a larger hole size allows more fluctuation at the constituent bonds. Thereby the multiple vacancies break little earlier even at low 10 K temperature. In a similar manner, the other orientations of the double and triple vacancy in armchair

tubes span the same cross-circumferential section and result in apparently similar strength. For zig-zag tubes the axial orientations differ 30 degrees which causes the non-reconstructed single vacancy and one orientation of double vacancy to result in similar strengths. The second pair is the remaining double vacancy orientation and a triple vacancy and the third, the weakest, is a triple vacancy in which the three missing atoms are along the circumferential zig-zag line of atoms.

It should be noted that increasing the temperature would add to the difference between the symbols corresponding to different vacancy orders because of increased fluctuations. Nevertheless, the results show clearly how the tensile strength varies with defect type and chirality and how large the relative drops in tensile strength are. Unlike the Young's modulus, the tensile strength is practically independent of tube diameter because in uniform axial loading the size and form of the defect define how much load the first-to-fail defect region bonds carry. A particular defect has practically the same form and orientation in tubes of same chirality but different diameter and thus the load has the same magnitude and spreads similarly in the bond region. There is a small diameter dependence visible in Fig. 4 due to smaller binding energy in thin tubes and slightly larger fluctuations.

## V. SUMMARY AND CONCLUSIONS

In this paper, we have studied theoretically the effects of vacancy-related defects on the mechanical characteristics of single-walled carbon nanotubes. Specifically, we have calculated the Young's modulus and tensile strength of SWNTs with vacancies for different defect concentrations and vacancy types.

We have found that the nanotube Young's modulus depends weakly on the vacancy concentration: a relatively high defect density of one vacancy per 50 Å gives rise to a small decrease in the Young's modulus: about 3 % only. Double and triple vacancies have a stronger effect on the modulus, but vacancy reconstructions by saturating dangling bonds diminish the degradation for the majority of the tubes and vacancy orientations studied.

We have further shown that vacancies have a much stronger effect on the tensile strength of nanotubes. Our simulations indicate that the tensile strength can degrade to 60 % of the intact tube value if vacancies are present. For the critical strain the effect can be even more deleterious. The critical strain of the defective SWNT can be half of the intact tube value. Similar to the nanotube Young's modulus, the degradation of tensile characteristics is partly alleviated by the ability of the nanotube carbon network to heal the vacancy damage by saturating the dangling bonds. However, even reconstructed defects decrease the tensile characteristics by $5-10$ % for the zig-zag tubes and $10-15$ % (tensile strength) and $25-30$ % (critical strain) for the armchair tubes. Overall, the tensile characteristics, especially if defects were present, were observed to be chirality dependent. This is consistent with the previous reports on tensile strength dependence on chirality for intact tubes [39].

These results indicate that the Young's modulus of nanotubes with defects will essentially be the same unless the vacancy concentration is extremely high. On the other hand, the tensile strength will substantially drop due to the quasi-one-dimensional atomic structure of SWNTs already if a single vacancy is present – the tensile strength of a SWNT is governed by the "weakest" segment of the tube. Given that a small number of defects are always present in nanotubes, this may explain why the theoretically predicted Young's modulus agrees well with the experimentally measured values, while the tensile characteristics are much worse.

Finally, within the framework of the continuum theory we have derived an expression which can be used to calculate the Young's modulus of defective CNTs at an arbitrary vacancy concentration, unless the defect concentration is so high that there are several defects in a specific nanotube unit cell. Thus, knowing the irradiation dose and defect production rate one can readily evaluate the drop in Young's modulus, which is indispensable for the qualitative explanation of the recent experimental data on the behavior of Young's modulus of irradiated nanotube bundles [24]. Note also that the defect concentration and ideally the defect types can be estimated by probing the electronic structure of nanotubes by using various experimental techniques such as Raman, electron spin resonance and optical absorption spectroscopy. Thus, simultaneous monitoring of the nanotube mechanical properties and defect concentration can shed light on the properties of irradiation-induced defects in carbon nanotubes.

Since our initial submission, similar results for the fracture behavior of nanotubes with defects have also been obtained [51] with the use of density functional theory, semiempirical methods and molecular mechanics.

### Acknowledgments

This work was supported in part by the Academy of Finland, Research Centre for Computational Science and Engineering, Project No. 44897 (Finnish Center of Excellence Program 2000-2005) and No. 50578. M.S. would also like to acknowledge GETA, Graduate School in Electronics, Telecommunications, and Automation, for funding.

[1] M. M. J. Treacy, T. W. Ebbesen, and J. M. Gibson, Nature **381**, 678 (1996).

[2] E. W. Wong, P. E. Sheehan, and C. M. Lieber, Science

**277**, 1971 (1997).
[3] P. Poncharal, Z. L. Wang, , D. Ugarte, and W. A. de Heer, Science **283**, 1513 (1999).
[4] A. Krishnan, E. Dujardin, T. W. Ebbesen, P. N. Yianilos, and M. M. J. Treacy, Phys. Rev. B **58**, 14013 (1998).
[5] J. P. Lu, Phys. Rev. Lett. **79**, 1297 (1997).
[6] E. Hernández1, C. Goze, P. Bernier, and A. Rubio, Phys. Rev. Lett. **80**, 4502 (1998).
[7] M.-F. Yu, O. Lourie, M. J. Dyer, K. Moloni, T. F. Kelly, and R. S. Ruoff, Science **287**, 637 (2000).
[8] A. B. Dalton, S. Collins, E. Munoz, J. M. Razal, V. H. Ebron, J. P. Ferraris, J. N. Coleman, B. G. Kim, and R. H. Baughman, Nature (London) **703**, 423 (2003).
[9] M. Cadek, J. N. Coleman, V. Barron, K. Hedicke, and W. J. Blau, Appl. Phys. Lett. **81**, 5123 (2002).
[10] A. H. Barber, S. R. Cohen, and H. D. Wagner, Appl. Phys. Lett. **82**, 4140 (2003).
[11] M. Terrones, F. Banhart, N. Grobert, J.-C. Charlier, H. Terrones, and P. Ajayan, Phys. Rev. Lett **89**, 075505 (2002).
[12] H. D. Wagner, Chem. Phys. Lett. **361**, 57 (2002).
[13] R. Andrews, D. Jacques, D. Qian, and E. C. Dickey, Carbon **39**, 1681 (2001).
[14] D. B. Mawhinney, V. Naumenko, A. Kuznetsova, J. T. Yates Jr., J. Liu, and R. E. Smalley, Chem. Phys. Lett. **324**, 213 (2000).
[15] N. Pierard, A. Fonseca, Z. Konya, I. Willems, G. Van Tendeloo, and J. B. Nagy, Chem. Phys. Lett. **335**, 1 (2001).
[16] B. Ni and S. B. Sinnott, Phys. Rev. B **61**, 16343 (2000).
[17] B. Ni, R. Andrews, D. Jacques, D. Qian, M. B. J. Wijesundara, Y. Choi, L. Hanley, and S. B. Sinnott, Applied. Physics A: Mater. Sci. Process. **105**, 12719 (2001).
[18] Y. Hu, I. Jang, and S. B. Sinnott, Compos. Sci. Technol. **63**, 1663 (2003).
[19] C. A. Cooper, S. R. Cohen, A. H. Barber, and H. D. Wagner, Appl. Phys. Lett. **81**, 3873 (2002).
[20] M.-F. Yu, B. S. Files, S. Arepalli, and R. S. Ruoff, Phys. Rev. Lett. **84**, 5552 (2000).
[21] C. Mikó, M. Milas, J. W. Seo, E. Couteau, N. Barisić, R. Gaál, and L. Forró, Appl. Phys. Lett. **83**, 4622 (2003).
[22] H. Stahl, J. Appenzeller, R.Martel, P. Avouris, and B. Lengeler, Phys. Rev. Lett. **85**, 5186 (2000).
[23] E. Salonen, A. V. Krasheninnikov, and K. Nordlund, Nucl. Instr. and Meth. in Phys. Res. B **193**, 603 (2002).
[24] A. Kis, G. Csányi, J.-P. Salvetat, T.-N. Lee, E. Couteau, A. J. Kulik, W. Benoit, J. Brugger, and L. Forró, Nat. Mat. **3**, 153 (2004).
[25] M. Huhtala, A. V. Krasheninnikov, J. Aittoniemi, K. Nordlund, and K. Kaski, Phys. Rev. B, in print **69** (2004).
[26] M. Terrones, H. Terrones, F. Banhart, J.-C. Charlier, and P. M. Ajayan, Science **288**, 1226 (2000).
[27] L. Shen and J. Li, Phys. Rev. B **69**, 045414 (2004).
[28] M. Arroyo and T. Belytschko, Phys. Rev. B **69**, 115415 (2004).
[29] C. Li and T.-W. Chou, Phys. Rev. B **69**, 073401 (2004).
[30] A. V. Krasheninnikov, K. Nordlund, M. Sirviö, E. Salonen, and J. Keinonen, Phys. Rev. B **63**, 245405 (2001).
[31] P. M. Ajayan, V. Ravikumar, and J.-C. Charlier, Phys. Rev. Lett. **81**, 1437 (1998).
[32] A. V. Krasheninnikov and K. Nordlund, J. Vac. Sci. Technol. B **20**, 728 (2002).
[33] A. V. Krasheninnikov, K. Nordlund, and J. Keinonen, Phys. Rev. B **65**, 165423 (2002).
[34] M. P. Allen and D. J. Tildesley, *Computer Simulation of Liquids* (Oxford University Press, Oxford, England, 1989).
[35] D. W. Brenner, Phys. Rev. B **42**, 9458 (1990).
[36] Y. Xia, Y. Ma, Y. Xing, Y. Mu, C. Tan, and L. Me, Phys. Rev. B **61**, 11088 (2000).
[37] M. B. Nardelli, B. I. Yakobson, and J. Bernholc, Phys. Rev. B **57**, 4277 (1998).
[38] H. J. C. Berendsen, J. P. M. Postma, W. F. van Gunsteren, A. DiNola, and J. R. Haak, J. Chem. Phys. **81**, 3684 (1984).
[39] T. Belytschko, S. P. Xiao, G. C. Schatz, and R. S. Ruoff, Phys. Rev. B **65**, 235430 (2002).
[40] B. I. Yakobson, M. P. Campbell, C. J. Brabec, and J. Bernholc, Comp. Mat. Sci. **8**, 341 (1997).
[41] T. Xiao and K. Liao, Phys. Rev. B **66**, 153407 (2002).
[42] C. Wei, K. Cho, and D. Srivastava, Appl. Phys. Lett. **82**, 2512 (2003).
[43] C. Wei, K. Cho, and D. Srivastava, Phys. Rev. B **67**, 115407 (2003).
[44] T. Dumitrica, T. Belytschko, and B. I. Yakobson, J. Chem. Phys. **118**, 9485 (2003).
[45] P. Zhang, P. E. Lammert, and V. H. Crespi, Phys. Rev. Lett. **81**, 5346 (1998).
[46] G. G. Samsonidze, G. G. Samsonidze, and B. I. Yakobson, Phys. Rev. Lett. **88**, 065501 (2002).
[47] M. B. N. Q. Zhao and J. Bernholc, Phys. Rev. B **65**, 144105 (2002).
[48] F. Banhart, Rep. Prog. Phys. **62**, 1181 (1999).
[49] A. A. El-Barbary, R. H. Telling, C. P. Ewels, M. I. Heggie, and P. R. Briddon, Phys. Rev. B **68**, 144107 (2003).
[50] R. W. Herzberg, *Deformation and Fracture Mechanics of Enigineering Materials* (John Wiley & Sons, Inc., USA, 1996).
[51] S. L. Mielke, D. Troya, S. Zhang, J. Li, S. Xiao, R. Car, R. S. Ruoff, G. C. Schatz, and T. Belytschko, Chem. Phys. Lett. **390**, 413 (2004).